Size-Dependent Selective Etching Mechanism: Cavity Formation on Barium Titanate Nanocubes

ARTICLE *in* THE JOURNAL OF PHYSICAL CHEMISTRY C · OCTOBER 2008

Impact Factor: 4.77 · DOI: 10.1021/jp8057993

4 AUTHORS, INCLUDING:

Duo Liu
Shandong University
47 PUBLICATIONS **1,126** CITATIONS
SEE PROFILE

Hong Liu
Shandong University
529 PUBLICATIONS **5,448** CITATIONS
SEE PROFILE

Article

Size-Dependent Selective Etching Mechanism: Cavity Formation on Barium Titanate Nanocubes

Shubin Qin, Duo Liu, Hong Liu, and Zhiyuan Zuo

J. Phys. Chem. C, **2008**, 112 (44), 17171-17174 • DOI: 10.1021/jp8057993 • Publication Date (Web): 09 October 2008

Size-Dependent Selective Etching Mechanism: Cavity Formation on Barium Titanate Nanocubes

Shubin Qin, Duo Liu,* Hong Liu, and Zhiyuan Zuo

State Key Laboratory of Crystal Materials, Shandong University, 27 South Shanda Road, Jinan, Shandong 250100, P. R. China

Received: June 10, 2008; Revised Manuscript Received: September 3, 2008

We report here the selective formation of nanosized cavities on barium titanate ($BaTiO_3$) nanocubes through a simple acid etching route in hydrothermal environment. Microstructural analysis reveals that the etching process is size dependent with small cavity preferentially formed on the nanocubes greater than a characteristic length of ~60 nm. A dislocation assisted etching mechanism is proposed to account for the experimental observations and discussed on the basis of the classical dislocation theory. This simple method could be extended to other perovskites for fabricating novel and complex ferroelectric nanostructures.

Introduction

Recent interests on the design and fabrication of nanodevices stem from the distinct and fascinating properties of nanostructured materials. Among those, ferroelectric nanostructures are of particular interests due to their high sensitivities and coupled responses to external inputs,[1] which facilitates their applications as ultrasensitive sensors and transducers. A major topic in modern ferroelectrics is to understand the effects of defects and their evolution under the influence of external conditions such as pressure, temperature, and synthesis conditions.[2] Although defects in ferroelectric perovskites such as oxygen vacancies, dislocations, and domain walls have been studied for decades, current understandings are limited to bulk and thin film ferroelectrics and are still not sufficiently enough to describe their behaviors at nanoscale. In view of the urgent requirement to integrate ferroelectric components into microdevices and enhanced size-dependent piezoelectricity for nanosized ferroelectric heterostructure,[3] it becomes essential to explore the etching behaviors of ferroelectric nanostructures and their microstructural aspects.

In this article, we present a study on the etching behaviors of $BaTiO_3$ nanocubes with well-defined shape and a narrow size distribution. Chemical etching of $BaTiO_3$ nanocubes was realized with hydrochloric acid under hydrothermal conditions. It is confirmed that the etching behaviors of $BaTiO_3$ nanocubes are size dependent; that is, larger nanocubes are more likely to be etched with nanosized cavities formed on their habit facets. In contrast, smaller nanocubes undergo the conventional Ostwald dissolution process. A dislocation assisted etching mechanism is proposed to account for this interesting observation.

Experimental Section

The barium titanate nanocubes studied were synthesized through a composite-hydroxide-mediated (CHM) approach reported elsewhere.[4] A mixture of 20 g of anhydrous hydroxides (NaOH/KOH = 51.5:48.5) was put into a 25 mL Teflon-lined autoclave, followed by addition of 0.6 mmol of $BaCl_2$ and 0.5 mmol of TiO_2 (anatase). The autoclave was then sealed and heated at 200 °C for 48 h. After reaction, the autoclave was taken out to allow cooling to room temperature. The intermediate product was dissolved, filtered and washed thoroughly with deionized water and diluted hydrochloric acid (0.05 M) to remove excessive hydroxide and barium carbonate. The final product was dried in vacuum overnight for further analysis. The etching process of $BaTiO_3$ nanocubes was carried out in an acidic solution (aqueous 1 M HCl) under hydrothermal conditions. As-synthesized $BaTiO_3$ nanocubes (50 mg) were mixed with 10 mL of 1 M HCl solution. The mixture was then transferred into a 25 mL Teflon-lined stainless autoclave. The autoclave was sealed, shaken and placed in an oven preset at 120 °C for 2.5 h. The temperature and reaction time reported here had been optimized to provide a more explicit illustration. Extended etching time leads to complete conversion of $BaTiO_3$ to spindle-shaped TiO_2 as verified by XRD and SEM. After reaction, the autoclave was taken out and the precipitation was collected by filtering and washing to remove excessive hydrogen ions until a pH value of 7 was reached. The microstructures of the as-synthesized and etched solid products were investigated by using powder X-ray diffractometer (XRD, Bruker D8 Advance, Cu Kα, Ni filter, $\lambda = 1.540598$ Å, 40 kV, 40 mA). Morphology was studied with field emission scanning electron microscopy (FESEM, Hitachi S-4800). High-resolution transmission electron microscopy (HRTEM) (Hitachi HF-2000 Field Emission Gun operating at 200 kV) was used to determine the crystallographic orientation and dislocation structures.

Results and Discussion

General. The formation mechanism of $BaTiO_3$ nanocubes synthesized through the CHM method has been discussed elsewhere and will not be repeated here.[4] The CHM method differs from hydrothermal synthesis on the fact that much less water is involved. Figure 1a shows the XRD pattern of the as-synthesized product. All the diffraction peaks can be indexed to tetragonal $BaTiO_3$ (*P4mm*, JCPD 81−2203). The slight asymmetric broadening of some diffraction peaks suggests that some particles may have cubic structure due to the well-known *ferroelectric size effect*.[5] The inset of Figure 2a shows a typical SEM image obtained on the as-synthesized product. It can be seen that all nanoparticles exhibit quasi-cubic morphology with a narrow size distribution of ~30−100 nm (therefore, will be

* To whom correspondence should be addressed. E-mail: liuduo@sdu.edu.cn.

10.1021/jp8057993 CCC: $40.75
Published on Web 10/09/2008

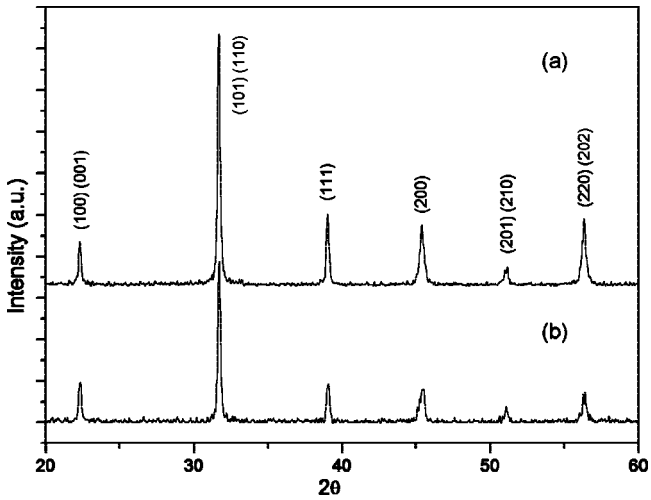

Figure 1. XRD patterns of $BaTiO_3$ nanocubes before (a) and after (b) hydrothermal treatment.

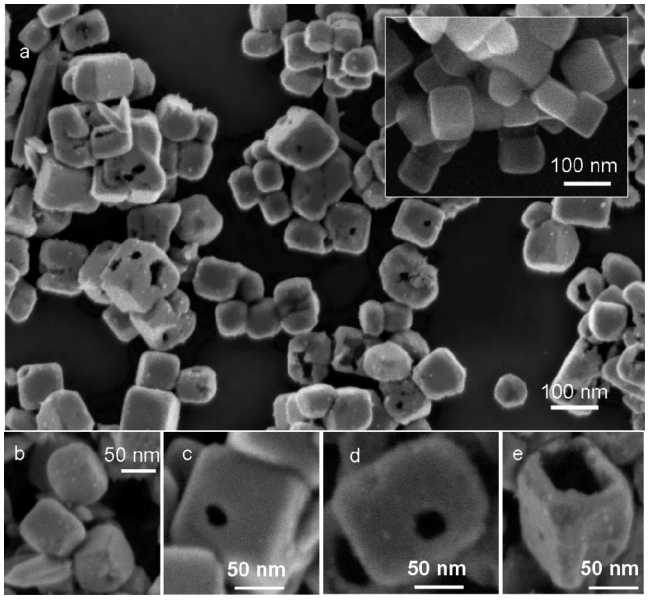

Figure 2. SEM image of $BaTiO_3$ nanocubes after hydrothermal etching (a) (inset: SEM image of $BaTiO_3$ nanocubes prior to hydrothermal etching). SEM image of $BaTiO_3$ nanocubes smaller than 60 nm after hydrothermal etching (b). SEM images of $BaTiO_3$ nanocubes greater than 60 nm but with different sizes (c) (d) and (e).

called nanocubes hereafter). It is known that hydrothermal $BaTiO_3$ tends to have hydroxyl (OH) groups incorporated in the lattice. Lattice OH groups are characterized by sharp IR absorption bands centered in a narrow range from 3462.5 to 3509.5 cm^{-1}.[6,7] FTIR analysis reveals that $BaTiO_3$ nanocubes synthesized through CHM approach contain much less lattice hydroxyl groups than hydrothermal $BaTiO_3$. This conclusion is also supported by FTIR analysis of $BaTiO_3$ nanocubes after thermal treatment at 800 °C for 1 h (an effective way for removing lattice OH groups[7]), where both FTIR curves for $BaTiO_3$ nanocubes before and after thermal treatment show analogous absorption behaviors from 3000 to 4000 cm^{-1}.

The etched product was also examined by XRD and SEM. The XRD pattern (Figure 1b) shows reduced diffraction intensities without visible variations on the peak positions. Figure 2a shows a typical SEM image of the etched product, which reveals similar size distribution to that of the as-synthesized product (the inset of Figure 2a). The difference lies on the fact that nanosized cavities are formed on some nanocubes. A statistical

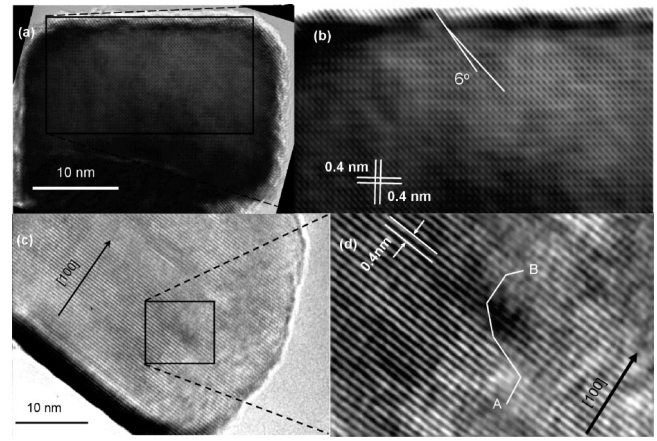

Figure 3. HRTEM images of $BaTiO_3$ nanocubes with different sizes shows lattice structures with (a) and without (c) dislocation. Images (b) and (d) are areas enlarged from image (a) and (c), respectively.

analysis of all SEM images for more than 100 etched nanocubes reveals that cavities can only be created on nanocubes greater than ~60 nm. The elongated particles in the upper left corner of Figure 2a are titania. $BaTiO_3$ nanocubes will be fully transformed to spindle-like titania (TiO_2) nanoparticles by extended acid treatment, as confirmed by XRD and SEM analyses. Figure 2b−e shows SEM images of nanocubes of different sizes after hydrothermal etching under the same experimental conditions. Figure 3b shows that nanocubes smaller than ~60 nm remain intact, while Figure 3c−e shows that cavities can be created on nanocubes greater than ~60 nm. The etching process was initiated on cube surfaces (Figure 2c) and can penetrate all the way through a nanocube (Figure 2e). This observation is also confirmed by TEM images. Figure 2d reveals a square-like cavity with edges oriented in the crystallographic [100] directions. In particular, the container-like structure is the first structure of this type ever being fabricated on perovskite that could be used to store molecules or small items (Figure 2e).

What seems unexpected is the fact that smaller nanocubes show a better chance to survive the acid attack and remain intact (Figure 2b), in controversy with the Ostwlad dissolution mechanism. According to the Gibbs−Thompson relation, the equilibrium solute concentration for nanoparticles can be described by

$$C(r,T)/C(\infty,T) = \exp\left(\frac{2\gamma V_m}{R} \cdot \frac{1}{rT}\right) \quad (1)$$

where $C(r,T)$ represents the equilibrium concentration for a nanoparticle with radius r at temperature T, $C(\infty,T)$ is the equilibrium bulk solubility, γ is the surface energy, and V_m is the molar volume. Within an individual nanocube, cube corners and edges correspond to large curvature and therefore enhanced chemical reactivity. As a result, the dissolution of the edges and corners is energetically favored, which yields the morphologies shown in Figure 2b. However, eq 1 also predicts that smaller nanocubes have higher dissolubility than larger ones. Consequently, they should dissolve first in compensation of the growth of larger ones. There arises the question: why etch pits are usually observed on larger nanocubes instead of smaller ones? Thus, in order to clarify this question, it is essential to study the lattice structure of the as-synthesized nanocubes.

HRTEM Analysis. Figure 3a shows a typical HRTEM image taken on a $BaTiO_3$ nanocube with length ~30 nm and width ~40 nm, respectively. It can be seen that the outside regions of

the nanocube are enclosed by (100) and (110) habit facets due to their lower surface energies and higher chemical stabilities.[8] The Moire pattern located at the lower left part of the image is due to the overlapping of another nanocube with the one of interest. Perfect lattice fringes free of dislocations or stacking faults can be clearly identified as shown in the enlarged fast Fourier transformation (FFT) filtered image (Figure 3b). A cautious examination of the regions not included in Figure 3b reveals the same result.

It can also be seen that the near-surface regions contain superstructure (~3−4 top surface layers) with distorted lattices that forms a deviation angle of ~6° with respect to the inside region. Obviously, defective layers with distinct lattice structures from $BaTiO_3$ were formed on the surfaces. Theoretical calculations by using first principles methods predicted that Ti−O interactions in $BaTiO_3$ are basically covalent, while unlike Pb−O bonds in $PbTiO_3$, the Ba−O interactions are essentially ionic. [9,10] Consequently, hydrothermal $BaTiO_3$ are usually nonstoichiometric with "TiO_2 character" in the near surface region due to the leaching of Ba^{2+} cations from the surface of $BaTiO_3$ to solution.[11,12]

The chemical reaction occurred during the growth process in solid−liquid interfaces could be written as a reversible reaction of this type:[13]

$$Ba^{2+}(aq) + Ti(OH)_4(aq) + 2OH^-(aq) \leftrightarrow BaTiO_3(s) + 3H_2O(l) \quad (2)$$

As can be seen, the chemical process consists of dehydration of $Ti(OH)_4$ and precipitation of Ti−O networks followed by diffusive incorporation of Ba^{2+} cations. This two-step mechanism results in the formation of covalent Ti−O octahedron network with "TiO_2 character" and thus distorted lattices.

As surface growth can be treated as interface reactions balanced between outward (precipitation) and inward (dissolution) processes,[14] the dissolution of $BaTiO_3$ in acid contains outward diffusion of Ba^{2+} cations followed by dissolution of Ti−O network. Accordingly, the diffusivity of Ba^{2+} cations and the solubility of TiO_2 in acidic environment are the rate determinant factors. Due to the reduced solubility of TiO_2 in acidic solutions than in basic solutions,[15] the Ti−O surface layers increase the diffusion path of Ba^{2+} ions and protect the internal regions from acid attack, thereby resulting in a reduced etching rate. As a result, the dissolution of smaller nanocubes is controlled mainly by thermodynamic aspects of the habit facets exposed to etchant and the Ti−O layers may retard the dissolution process. It should be noted that the surface of the cavities may also contain Ti−O layers that may suppress the dielectric and ferroelectric properties of $BaTiO_3$.

In contrast, stress concentrators such as dislocations are characterized by distorted lattices and enhanced chemical reactivity, which results in preferential removal of adjacent atoms along dislocation lines to form etch pits. Figure 3c shows a HRTEM image obtained on a nanocube with size ~60 nm. The enlarged FFT image (Figure 3d) clearly shows dislocation outlets and stacking faults (marked by white lines with A and B denoting the dislocation outlets). Perovskites are characterized by high tolerance to lattice distortion, forming the foundation of many fascinating properties. Two types of dislocations with Burgers vectors $[100]_{pc}$ and $[110]_{pc}$ (subscript pc denotes pseudocubic and will be omitted for convenience hereafter) have been experimentally verified in perovskites such as $KZnF_3$, $CaTiO_3$, $BaTiO_3$, and $SrTiO_3$.[16] For a typical perovskite structure, where the shortest lattice burgers vector is {100}-type, dislocation loop is characterized as a burgers vector of <100> lying on the {100} plane. However the <100> dislocation is energetically unfavorable due to the low packing density and ionic repulsion.[17] It therefore tends to dissociate to two partial dislocations given as $<100> \rightarrow 1/2<110> + 1/2<1\bar{1}0>$,[18,19] which produces the image shown in Figure 3d. Obviously, the surface dislocations are subjected to image forces that tend to drive them out of the nanocube through slip or glide. However, the heavily strained top Ti−O layers could shield the image forces excreted on dislocations, which along with lattice friction (the Peierls stress) restricts the motion of the dislocations. As a result, dislocations and stacking faults are usually observed in regions not exactly located at the center of the nanocubes.

Although point defects such as oxygen vacancies and hydroxyl groups may also increase local etching rate, their effects are highly localized and, if there are any, should be observable on all nanocubes no matter they are greater or smaller than 60 nm. Direct experimental evidence are provided by etching $BaTiO_3$ nanocubes sintered at 800 °C for 1 h to remove hydroxyl groups. It can be seen that etch pits can also be formed on the sintered $BaTiO_3$ nanocubes by acid etching, similar to the as-synthesized product. As a result, lattice hydroxyl groups are excluded as the primary origins responsible for the etch pits shown in Figure 2 and lattice dislocations or stacking faults have to be considered. Note that dissolution of highly strained regions around dislocation lines could form either straight (in the case of pure dislocations) or twisted (in the case of mixed dislocations) etching paths, which could produce the morphologies shown in Figure 2a.

Discussion on Dislocations. The classical elastic theory predicts a characteristic length below which dislocation can not exist within an isolated nanoparticle that has properties dramatically different from their dislocated counterparts in ways such as mechanical properties, chemical stability, electronic and ionic conductivity, and band gap.[20,21] Previous studies on nanocrystalline particles suggested that lattice dislocations could leave crystals spontaneously when the crystal size is less than a characteristic length given by[22,23]

$$A_c \cong {}^{2Gb}/_{\sigma_p} \quad (3)$$

where G is the shear modulus, b is the Burgers vector of the dislocation, and σ_p is the Peierls stress (the minimum stress required to move a dislocation one lattice parameter). The Peierls stress was originally given by Peierls and Nabbarro and had been recently improved by Joos and Duesbery in a more precise manner for narrow width dislocations given by[24]

$$\sigma_p = \frac{3\sqrt{3}}{2}\frac{a(1-\upsilon)}{Gb}\tau_{\max}^2 \quad (4)$$

where G is the shear modulus of the material, a the lattice parameter, b the Burgers vector, υ the Poisson ratio, and τ_{max} the ideal shear strength. Taking an average shear modulus of 55 GPa for $BaTiO_3$ single crystal,[25] Burgers vector $b = a[110]/2 = 0.28$ nm, and the ideal shear strength of 5.5 GPa, [26] σ_p and A_c for spherical $BaTiO_3$ nanoparticles are estimated to be ~1.4 GPa and ~22 nm, respectively. The calculated A_c (~22 nm) is much smaller than the value determined by SEM analyses due to the combined effects of the following factors: (1) the assumption of spherical shape used for the development of the original model for the characteristic length, (2) the elastic anisotropy (an anisotropic factor of ~2.5) of $BaTiO_3$, (3) the sink of dislocations in the Ti−O surface layers. Although size effect on elastic properties is expected to be negligible for nanoparticles greater than 10 nm, [27] its implication becomes

much more complicated for $BaTiO_3$ whose phase transition temperature (the Curie point) has been found to be size dependent (the so-called *ferroelectric size effect*). The structural transition to cubic phase may lead to dramatic changes of the shear modulus and Poissons' ratio, thereby altering the characteristic length. In order to clarify this issue, ab initio calculation was performed on $BaTiO_3$ with the built- in CASTEP module of Material Studio by assuming a cubic symmetry with lattice parameters of 0.4 nm, the computed elastic stiffness constants are as follows. $C_{11} = 284.9$ GPa, $C_{12} = 110.8$ GPa, C_{44} (shear modulus, G) $= 116.2$ GPa. The computed C_{12} and C_{44} agree well with experimental values, while C_{11} is $\sim$10% greater than the experimental value. [28] Inserting C_{44} to eq 3 yields a characteristic length of 46.5 nm for cubic $BaTiO_3$ (approximately twice of the tetragonal $BaTiO_3$), suggesting that ferroelectric size effect can not be ignored on describing the etching behaviors of $BaTiO_3$ nanocubes. However, this value is still smaller by 23% than the characteristic length ($\sim$60 nm) obtained by SEM analysis. As a consequence, a detailed description of the etching behaviors of $BaTiO_3$ nanocubes requires an in-depth analysis of Ti−O surface layers, elastic anisotropy, and particle geometry, not presently available.

Conclusions

In summary, nanosized cavities are successfully fabricated on $BaTiO_3$ nanocubes via a simple hydrothermal etching route. It is verified that dislocation-free $BaTiO_3$ nanocubes undergo the classical Ostwald dissolution process, while preferential etching occurs on their dislocated counterparts. This size dependent etching mechanism has potential to be extended to other perovskites for fabricating complex functional nanostructures. Future work involves nanoscale investigation of ferroelectricity for this novel nanostructure.

Acknowledgment. The authors thank National Science Foundation of China (NSFC) through Grant No. 50702031, National Basic Research Program of China (973 Program) through Grant No. 2009CB930503, and the Program of Introducing Talents of Discipline to Universities in China (111 program) for financial support.

References and Notes

(1) Scott, J. F. *Science* **2007**, *315*, 954–959.
(2) Damjanovic, D. *Rep. Prog. Phys.* **1998**, *61*, 1267–1324.
(3) Majdoub, M. S; Sharma, P.; Cagin, T. *Phys. Rev. B* **2008**, *77*, 125424−1125424−9.
(4) Liu, H.; Hu, C.; Wang, Z. L. *Nano Lett.* **2006**, *6*, 1535–1540.
(5) Frey, M. H.; Payne, D. A. *Phys. Rev. B* **1996**, *54*, 3158–3168.
(6) Kapphan, S.; Weber, G. *Ferroelectrics* **1981**, *37*, 673–676.
(7) Noma, T.; Wada, S.; Mamoru, Y.; Suzuki, T. *J. Appl. Phys.* **1996**, *80*, 5223.
(8) Eglitis, R.; Borstel, I. G.; Heifets, E.; Piskunov, S.; Kotomin, E. *J. Electroceram.* **2006**, *16*, 289–292.
(9) Salehi, H.; Hosseini, S. M; Shahtahmasebi, N. *Chin J. Phys.* **2004**, *42*, 619–628.
(10) Xue, X. Y.; Wang, C. L.; Zhong, W. L. *Surf. Sci.* **2004**, *550*, 73–80.
(11) Clark, I. J.; Takeuchi, T.; Ohtori, N.; Sinclair, D. C. *J. Mater. Chem.* **1999**, *9*, 83–91.
(12) Blanco-Lopez, M. C.; Rand, B.; Riley, F. L. *J. Eur. Ceram. Soc.* **1997**, *17*, 281–287.
(13) Testino, A; Buscaglia, V; Buscaglia, M. T.; Viviani, M.; Nanni, P. *Chem. Mater.* **2005**, *17*, 5346–5356.
(14) Tong, W. M.; Williams, R. S. *Annu. Rev. Phys. Chem.* **1994**, *45*, 401–438.
(15) Okada, K.; Yanagisawa, T.; Kameshima, Y.; Nakajima, A. *Mater. Res. Bull.* **2007**, *42*, 1921–1929.
(16) Cordier, P.; Ungar, T.; Zsoldos, L.; Tichy, G. *Nature.* **2004**, *428*, 837–840.
(17) Suzuki, T.; Ueno, M.; Nishi, Y.; Fujimoto, M. *J. Am. Ceram. Soc.* **2001**, *84*, 200–206.
(18) Doukhan, N.; Doukhan, J. C. *Phys. Chem. Miner.* **1986**, *13*, 403–410.
(19) Poirier, J. P.; Peyronneau, J.; Gesland, J. Y.; Brebec, G. *Phys. Earth Planet. Inter.* **1983**, *32*, 307–312.
(20) Siegel, R. W. *Annu. Rev. Mater. Sci.* **1991**, *21*, 559–578.
(21) Madhukar, A.; Lu, S. Y.; Konker, A.; Ho, M.; Hughes, S. M.; Alivisatos, A. P. *Nano Lett.* **2005**, *5*, 479–482.
(22) Narayan, J *J. Appl. Phys.* **2006**, *100*, 034309(1)-034309(5).
(23) Gryaznov, V. G; Polonsky, I. A.; Romanov, A. E.; Trusov, L. I. *Phys. Rev. B* **1991**, *44*, 42–46.
(24) Joos, B.; Duesbery, M. S. *Phys. Rev. Lett.* **1997**, *78*, 266–269.
(25) Watt, J. P.; Peselnick, L. *J. Appl. Phys.* **1980**, *51*, 1525–1531.
(26) Liu, D.; Chelf, M.; White, K. W. *Acta Mater.* **2006**, *54*, 4525–4531.
(27) Sharma, P.; Ganti, S. *J. Mater. Res.* **2003**, *18*, 1823–1826.
(28) Hellwege, K.-H, Ed. *Landolt-Bornstein: Numerical Data and Functional Relationships in Science and Technology*, New Series, Group III, Vols. *11* and *18*; Springer-Verlag: Berlin, 1979 and 1984.

JP8057993